One-pot biocatalytic transformation of adipic acid to 6-aminocaproic acid and 1,6-hexamethylenediamine using carboxylic acid reductases and transaminases

Fedorchuk, Tatiana P.; Khusnutdinova, Anna N.; Evdokimova, Elena; Flick, Robert; Di Leo, Rosa; Stogios, Peter J.; Savchenko, Alexei; Yakunin, Alexander

Journal of the American Chemical Society

DOI:
10.1021/jacs.9b11761

Published: 15/01/2020

Peer reviewed version

One-pot biocatalytic transformation of adipic acid to 6-aminocaproic acid and 1,6-hexamethylenediamine using carboxylic acid reductases and transaminases

Tatiana P. Fedorchuk[1,2#], Anna N. Khusnutdinova[1,2#], Elena Evdokimova[1], Robert Flick[1], Rosa Di Leo[1], Peter Stogios[1], Alexei Savchenko[1,3], and Alexander F. Yakunin[1,4*]

[1] Department of Chemical Engineering and Applied Chemistry, University of Toronto, Toronto, Ontario, M5S 3E5, Canada

[2] Institute of Basic Biological Problems, Russian Academy of Sciences, Pushchino, Moscow region, 142290, Russia

[3] Department of Microbiology, Immunology and Infectious Diseases, University of Calgary, Alberta, T2N 4N1, Canada

[4] Centre for Environmental Biotechnology, School of Natural Sciences, Bangor University, Gwynedd LL57 2UW, UK

[#] These authors contributed equally to this work.

* Corresponding author: a.iakounine@utoronto.ca; a.iakounine@bangor.ac.uk

ABSTRACT

Production of platform chemicals from renewable feedstocks is becoming increasingly important due to concerns on environmental contamination, climate change, and depletion of fossil fuels. Adipic acid (AA), 6-aminocaproic acid (6-ACA) and 1,6-hexamethylenediamine (HMD) are key precursors for nylon synthesis, which are currently produced primarily from petroleum-based feedstocks. In recent years, the biosynthesis of adipic acid from renewable feedstocks has been demonstrated using both bacterial and yeast cells. Here we report the biocatalytic conversion/transformation of AA to 6-ACA and HMD by carboxylic acid reductases (CARs) and transaminases (TAs), which involves two rounds (cascades) of reduction/amination reactions (AA → 6-ACA → HMD). Using purified wild type CARs and TAs supplemented with cofactor regenerating systems for ATP, NADPH, and amine donor, we established a one-pot enzyme cascade catalyzing up to 95% conversion of AA to 6-ACA. To increase the cascade activity for the transformation of 6-ACA to HMD, we determined the crystal structure of the CAR substrate-binding domain in complex with AMP and succinate and engineered three mutant CARs with enhanced activity against 6-ACA. In combination with TAs, the CAR L342E protein showed 50-75% conversion of 6-ACA to HMD. For the transformation of AA to HMD (via 6-ACA), the wild type CAR was combined with the L342E variant and two different TAs resulting in up to 30% conversion to HMD and 70% to 6-ACA. Our results highlight the suitability of CARs and TAs for several rounds of reduction/amination reactions in one-pot cascade systems and their potential for the bio-based synthesis of terminal amines.

INTRODUCTION

Polymers and their precursors constitute the largest fraction of all chemical products manufactured today. The global polymer market was valued at USD 522.7 billion in 2017 and is expected to grow at 4.0% annually over 2019-2025 (Grand View Research). The fastest growing polymer markets include polyamides and polyesters, with compound annual growth (CAGR) up to 8% [1]. In addition, worldwide demand for biobased polymers is quickly increasing, mostly driven by reduction of carbon footprints, switching to renewable feedstocks, and rising consumer awareness concerning sustainability issues [1-4]. Since the functional groups of polyamide and polyester precursors (amino, carboxyl, and hydroxyl) are common to the biological world, their total synthesis by biocatalysis or fermentation can be expected to be feasible. The global bio-polyamide market was valued at USD 110.5 million in 2016, and is projected to increase at a CAGR of 12.9% from 2017 to 2025 (Grand View Research, online report 2017) [1-2]. Nylon-6 and nylon-6,6 account for appr. 90% of the total amount of nylon produced today (worldwide nearly 7 million tons annually) [1]. Nylon-6 is a homopolymer of 6-aminocaproic acid (6-ACA), whereas nylon-6,6 is a co-polymer of two alternating building blocks, adipic acid (AA) and 1,6-hexamethylenediamine (HMD) (Figure 1). AA and 6-ACA are synthesized using chemical catalysis from benzene (via cyclohexane) and caprolactam, respectively, whereas HMD is predominantly produced by Ni-catalyzed hydrocyanation of 1,3-butadiene [5-7]. Currently, almost all polymer building block chemicals are produced using petroleum-based chemical processes, which are inherently non-sustainable and have detrimental impacts on the environment [1-4]. Thus, there is an

increasing global demand to replace petroleum-based chemical processes with bio-based chemical production from renewable resources.

Bio-based production of AA has been demonstrated using fatty acids, glucose, and glycerol as renewable feedstocks in *Escherichia coli*, yeast, and *Thermobifida fusca*,expressing engineered or natural (*T. fusca)* biosynthetic pathways [8-17]. Depending on the pathway and host used, these processes produced from 3 mg/L to 68 g/L of AA [2, 4]. Biosynthesis of ACA was achieved using *E. coli* cells expressing the α-ketoacid decarboxylase KdcA from *Lactococcus lactis* and aminotransferase Vfl from *Vibrio fluvialis*, with the ACA titer up to 160 mg/L [2, 18]. Although several patents propose various non-natural metabolic pathways for HMD biosynthesis [2], bio-based production of this commodity chemical from renewable feedstocks has not yet been realized. Thus, further efforts are required to establish and improve the bio-based production of 6-ACA and HMD.

Recently, carboxylic acid reductases (CARs) have emerged as attractive biocatalysts for biotransformation of organic acids to various chemicals [19-22]. In the presence of ATP and NADPH, CARs catalyze the reduction of carboxylic acids to an aldehyde [23]. These large enzymes (over 1,000 amino acids) have three domains: an N-terminal Adenylation (A) domain fused via a PCP-domain (Peptidyl Carrier Protein, a phosphopantetheine attachment site) to a C-terminal Reductase (R) domain (Figure S1) [24-25]. The recombinant CAR from *Nocardia iowensis* required post-translational activation (phosphopantetheinylation) by a phosphopantetheinyl transferase [25]. The CAR A-domain catalyzes the initial reaction between ATP and a substrate acid to form an acyl-AMP intermediate, which is then attacked by the phosphopantetheine thiol forming a

covalently bound acyl-thioester with the release of AMP [25]. The acyl-thioester phosphopantetheine then swings from the A-domain to the R-domain resulting in the reduction of the thioester by NADPH and producing the aldehyde product [23, 25-26]. Crystal structures of A-PCP and PCP-R di-domains from *N. iowensis* and *Segniliparus rugosus* revealed large-scale domain motions during the catalysis with two different conformations of the active site region (the "on" and "off" states) [27].

Purified recombinant CARs have been shown to accept a broad range of substrates including aromatic and aliphatic carboxylic acids [28-29]. Several successful applications of CARs have already been demonstrated for the production of alkanes, aromatic aldehydes, and chiral amines [19-20, 29-33]. Highly efficient one-pot enzyme cascades for the biosynthesis of chiral piperidines and pyrrolidines or for biocatalytic N-alkylation of amines have been developed using CAR, transaminase (TA), imine reductase, and reductive aminase biocatalysts [34-36]. TAs are pyridoxal-5′-phosphate (PLP) dependent enzymes that belong to the PLP fold types I (*S*-selective) and IV (*R*-selective) [37-39]. These enzymes catalyze the transfer of an amino group between an amine donor (different amino acids and amines) and an amine acceptor (a ketone or aldehyde). Of particular interest are ω-transaminases (ωTAs) which do not require the presence of a carboxylic group in substrates and can accept a large variety of carbonyl substrates [39]. Over the past decade, TAs have attracted considerable interest in biocatalysis both as individual biocatalysts and as part of multienzyme cascades for the synthesis of various amines [38-41].

In our recent work, we identified several bacterial CARs with robust activity toward both aromatic and aliphatic substrates [42]. Substrate screening of purified CARs against a panel of monocarboxylic acids revealed that these enzymes showed significant reductase

activity against C3-C10 substrates with the maximal activity toward C5-C7 substrates [42]. In addition, the subgroup II CARs, MAB4714 from *Mycobacterium abscessus* and MCH22995 from *M. chelonae*, exhibited significant activity against AA (C6), 7-aminoheptanoic acid (C7), and 8-aminooctanoic acid (C8), suggesting that some CARs can tolerate the presence of the second charged group in substrates. Purified CARs supplemented with cofactor regenerating systems (for ATP and NADPH) and an aldo-keto reductase (AKR) catalyzed up to 76% conversion of AA to 1,6-hexanediol (Figure 1) [42]. Here we explored the biotransformation of AA to 6-ACA (Cascade-1) and then to HMD (Cascade-2) using CARs and ωTAs (Figure 1). When supplemented with cofactor regenerating systems, the wild type CAR and ωTA demonstrated up to 95% substrate conversion in the *in vitro* transformation of AA to 6-ACA (Cascade-1) but showed low activity in the bioconversion of 6-ACA to HMD (Cascade-2). To enhance CAR activity toward 6-ACA, the crystal structure of its substrate-binding domain was determined in complex with AMP and succinate and used for structure-based protein engineering. Three mutant variants were found to exhibit enhanced activity against 6-ACA, as well as toward 7-aminoheptanoic acid and 8-aminooctanoic acid. In combination with ωTAs, the CAR L342E mutant protein showed up to 80% conversion of 6-ACA to HMD (Cascade-2). With AA as substrate, the mixture of the CAR wild type and L342E proteins and two ωTAs demonstrated up to 30% conversion to HMD and 70% to 6-ACA.

MATERIALS AND METHODS

Gene cloning and protein purification. The genes encoding CARs (MAB4714 and MCH22995), TAs, and other enzymes used in this work (Table S1) were amplified by

PCR using corresponding genomic DNA and cloned into a modified p15TVLic vector (Novagen) containing an N-terminal 6His-tag as described previously [43]. The *E. coli* inorganic pyrophosphatase PPA was expressed and purified using a clone from the *E. coli* ASKA collection [44]. The phosphopantetheinyl transferase (PPT) BSU03570 (Sfp) from *Bacillus subtilis* was cloned into a pCDFDuet plasmid without a 6His-tag for co-expression with CARs. Site-directed mutagenesis of the *Mycobacterium abscessus* CAR (MAB4714) and formate dehydrogenase (FDH) from *Pseudomonas* sp. strain 101 were performed using the QuikChange™ site-directed mutagenesis kit (Stratagene) according to the manufacturer's protocol, and the mutations were verified by DNA sequencing. All plasmids were transformed into the *E. coli* BL21(DE3) Gold strain (Agilent). Cells were grown in 1 L TB cultures, induced with 0.4 mM IPTG overnight at 16°C (or at 26°C for CARs). Recombinant proteins were purified to near homogeneity (>95%, Figure S2) using Ni-chelate affinity chromatography on Ni-NTA Superflow resin (Qiagen) as described previously [45]. The multiple sequence alignment was prepared using the MAFFT online tool and STRAP web server [46-47].

Enzymatic assays. Carboxylate reductase activity against different carboxylic acids was determined spectrophotometrically using an NADPH oxidation-based assay by following the decrease in absorbance at 340 nm. CAR assays were performed in a reaction mixture (0.2 ml) containing HEPES-K (100 mM, pH 7.5), 1 mM NADPH, 2.5 mM ATP, 10 mM $MgCl_2$, substrates (10 mM of aliphatic acids and 2 mM of cinnamic or benzoic acids), and 5-10 μg of purified CAR. Transaminase activity was determined in coupled reaction with alanine dehydrogenase (Ala-DH) BSU31930 or glutamate dehydrogenase (Glu-DH) GDH1 spectrophotometrically using an NAD(P)H oxidation-

based assay by following the decrease in absorbance at 340 nm (adapted from Wilding et al.[48]). Transaminase screens were carried out in a reaction mixture (0.2 ml) containing 100 mM HEPES-K (pH 7.5), 0.5 mM NADPH or NADH, 1 mM adipaldehyde, 0.05 mM PLP, 50 mM NH_4Cl, 2 mM Ala, 2 mM Glu, 5 µg of purified aminotransferases, 2.5 µg of Ala-DH, and 2.5 µg of Glu-DH. To determine kinetic parameters of enzymes (K_m and k_{cat}), microplate-based assays were performed (in triplicate) using a SpectraMax M2 plate-reader in a reaction mixture containing a range of variable substrates at 30°C. Kinetic parameters were determined by non-linear curve fitting from Michaelis-Menten plots using GraphPad Prism (version 5.00 for Windows, GraphPad Software, San Diego, CA).

Identification of reaction products. The reaction products of bioconversion reactions catalyzed by CARs and TAs (6-ACA and HMD) were quantified on a Varian ProStar HPLC system equipped with a fluorescence detector and C18 column (Pursuit 5 150×3.9 mm; Agilent Technologies, USA) using a modified protocol described previously [49]. After filtering through 10 kDa spin filters (PES membrane, VWR), 20 µl of reaction mixture was mixed with 5 µl of 0.3 M EDTA/0.44 M NaOH and 20 µl 0.5 M NaOH (for pH adjustment). For product derivatization, freshly prepared ortho-phthalaldehyde (OPA) (100 µl of 38.5 mM stock dissolved in 25% methanol (v/v), 10 mM Na_2SO_3, and 0.2% formaldehyde (v/v)) was added to 25 µl of reaction mixture (after pH adjustment), incubated for 1 min at 37°C (1,000 rpm), and centrifuged for 1 min at 13,000 rpm (Microfuge 22R Centrifuge, Beckman Coulter, USA). 20 µl aliquots of derivatized reaction mixture were injected immediately into the column, and products were resolved using the following elution gradient: 0–27 min: 30% solvent A, 70%

solvent B; 27–28 min: 0% A, 100% B; 28–30 min: 0% A, 100% B, followed by column equilibration with 80% solvent A, 20% solvent B. Solvent A was methanol:acetonitrile:water mix (45:45:10 ratio), and solvent B: 40 mM disodium perphosphate (Na_2HPO_5), 0.01% NaN_3 (pH 7.0, flow rate 0.7 ml min^{-1}, 26°C, detection wavelength: 340 nm excitation and 455 nm emission) (representative HPLC chromatograms are shown in Figure S3). Product concentrations were determined using linear regression analysis of peak areas. Calibration curves were prepared using different concentrations of 6-ACA and HMD. Results presented are means ± SEM (standard error of mean) from at least three independent determinations.

Liquid chromatography-mass spectrometry (LC-MS) analysis of reaction products (6-ACA and HMD) was performed using a Dionex Ultimate 3000 UHPLC system and a Q-Exactive mass spectrometer equipped with a HESI-II probe (all from Thermo Scientific) and controlled by Thermo XCalibur 4.1 software. LC separation was conducted on a Hypersil Gold C18 column (50 mm × 2.1 mm, 1.9 μm particle size, Thermo Scientific) equipped with a guard column, column temperature 40°C. Solvent A was 0.1% formic acid (in water), solvent B was 0.1% formic acid in methanol (flow rate 0.2 ml/min). Autosampler temperature was maintained at 8°C, and injection volume was 10 μl. The gradient was 0–1.5 min: 100% A; 1.5–7.0 min: 0% A, 100% B; 10–11 min: 100% A, 0% B; 11.0–15.0 min: 100% A. Data collection was done in positive ionization mode with a scan range *m*/*z* 90–200, resolution 140 000 at 1 Hz, AGC target of 3e6 ions and a maximum injection time of 250 ms. Standard solutions of HMD (*m*/z 117.1386) and 6-ACA (*m*/*z* 132.1019) were used for validation of retention time and *m*/*z*.

***In vitro* biotransformation of carboxylic acids by CARs and ωTAs.** *In vitro* biotransformations using MAB4714 and ωTAs (SAV2585 and/or PatA) in the presence of cofactor regenerating systems were performed in reaction mixtures (0.2 ml) containing 100 mM HEPES-K buffer (pH 7.5), 10 mM substrate (AA or 6-ACA), 2 mM NADPH, 2 mM L-Glu, 2 mM ATP, 5 mM polyP, 10 mM $MgCl_2$, 0.05mM PLP, 100 mM Na-formate, 50 mM NH_4Cl, 20 μg of CHU0107 (PPK2), 20 μg of the FDH D222Q/H224N double mutant protein, 20 μg of the *E. coli* inorganic pyrophosphatase (PPA), 20 μg of Glu-DH, 80 μg of CAR, and 20 μg of purified aminotransferases PatA or SAV2585 (overnight incubation at 30°C, 1,000 rpm). The *E. coli* inorganic pyrophosphatase PPA was added to the reaction to prevent inhibition of CAR activity by pyrophosphate produced during the CAR reaction [42, 50]. For reactions with Ala-dependent aminotransferases (RHA07987, SM5064, and SPO3471), the wild-type FDH (20 μg) and NADH (2 mM) were used in the reaction. After 12 h incubation, the reaction mixtures were filtered through 10 kDa centrifugation filters (PES membrane, VWR), and the reaction products were analyzed using HPLC or LC-MS.

Protein Crystallization and Crystal Structure Determination. 16 A domain fragments of 11 CARs (636-661 aa) were cloned into a pMCSG53 vector and expressed in *E. coli* BL21(DE3)-Gold cells as 6His-tagged proteins with a TEV cleavage site. 12 clones were found to produce soluble proteins, from which five proteins were purified for crystallization using metal-chelate affinity chromatography as described previously [42]. The crystals of the MCH22995 A domain (1-641 aa) were obtained by co-crystallization and the sitting drop method using 20 mg/mL protein, 2.5 mM adipic acid, 1 mM AMP-PNP and the reservoir solution 1.5 M lithium sulfate and 0.1 M Tris-HCl (pH 8.5).

Crystals were cryo-protected using 25% (w/v) ethylene glycol prior to flash freezing in a nitrogen stream. X-ray diffraction data were collected using a home source Rigaku HF-007 rotating anode and Rigaku R-AXIS IV detector. Diffraction data were reduced using HKL-3000 [51]. The structure was solved by Molecular Replacement (MR) using Phenix.phaser [52], and the MCH22995 A domain model was built using Phyre2 [53] and the structure of the A domain of the *Nocardia iowensis* carboxylate reductase (PDB 5MSD) [27]. The model was rebuilt using Phenix.autobuild, followed by manual model building and refinement with Coot [54] and Phenix.refine. AMP and succinate were built into residual F_o-F_c density in the active site of the enzyme after completion of protein model building. B-factors were refined and TLS parameterization was included in final rounds of refinement. Geometry was verified using Phenix and the wwPDB server. To generate the energy-minimized models of the MCH22995 A domain mutants (L345E, G421E, and A429W), these mutants were made in Coot and a sphere of 8 Å around succinate was energy minimized using YASARA (and default parameters). The crystal structure of the MCH22995 A-domain was deposited to the Protein Databank with accession number 6OZ1 (Table S2). Nucleotide sequences of plasmids used for protein over-expression and purification are presented in Table S3.

RESULTS AND DISCUSSION

Screening of purified ωTAs with adipaldehyde as substrate. The proposed bioconversion of adipic acid (AA) to 6-aminocaproic acid (6-ACA) and 1,6-hexamethylenediamine (HMD) using carboxylic acid reductases (CARs) and ω-transaminases (ωTAs) includes two cascades (AA → 6-ACA → HMD) producing several

aldehyde intermediates (adipic semialdehyde, adipaldehyde, and 6-aminohexanal), which serve as substrates for transaminases (Figure 1). Since adipic semialdehyde is not commercially available, we used adipaldehyde as a substrate to screen purified ωTAs for amination activity (Figure 1). For this screening, we selected 26 bacterial ωTAs from the Pfam families PF00202 (class III) and PF00155 (classes I and II), which were found to be expressed as soluble proteins in *E. coli* (Table S1). Purified proteins were screened for adipaldehyde amination activity using an enzyme-coupled NAD(P)H-oxidation assay with Glu-DH, Ala-DH and a mixture of L-Glu and L-Ala as amine donors. Significant adipaldehyde amination activity was observed in several enzymes including SM5064 from *Sinorhizobium meliloti*, SPO3471 from *Ruegeria pomeroyi*, SAV2585 from *Streptomyces avermitilis*, and *E. coli* GabT and PatA (Figure S4). Further biochemical characterization of the six most active enzymes with adipaldehyde revealed that they can use L-Glu (GabT, PatA, and SAV2585) or L-Ala (RHA07987, SM5064, and SPO3471) as amine donors with K_m for adipaldehyde in the range 0.1 – 1.3 mM and k_{cat} = 0.1 – 1.2 s^{-1} (Table 1). Thus, we identified several transaminases active toward adipaldehyde, which can be used in combination with CARs for biotransformation of adipic acid to 6-ACA and HMD.

Cofactor regenerating systems for bioconversion of adipic acid using CARs and ωTAs. CARs and ωTAs consume ATP, NADPH, and amine donor (L-Ala or L-Glu) during biotransformation of adipic acid to 6-ACA and HMD (Figure 2). A common strategy to reduce the high costs of cofactor-driven *in vitro* biotransformations is the use of cofactor regenerating systems [55-57]. Recently, we established a polyphosphate-based regenerating system for the regeneration of ATP from AMP [42]. This system is based on

the activity of the family-2 polyphosphate kinase (PPK2) CHU0107 from *Cytophaga hutchinsonii*, which catalyzes polyphosphate (polyP)-dependent phosphorylation of AMP to ATP (via ADP) and exhibits high activity and affinity to AMP, ADP, and polyP [58]. For the regeneration of pyridine nucleotides ($NADP^+$ and NAD^+), several enzymatic reactions have been proposed including phosphite dehydrogenase, glucose-6-phosphate dehydrogenase, glucose dehydrogenase, and formate dehydrogenase [55-57]. For NADH regeneration in this work, we selected the wild type formate dehydrogenase (FDH) from *Pseudomonas* sp. strain 101 (Uniprot ID P33160), which preferentially reduces NAD^+ to NADH using formate as reductant and producing CO_2 [59]. For NADPH regeneration, we introduced two mutations into FDH (D222Q and H224N) producing a mutant FDH enzyme (D222Q/H224N) with a preference to $NADP^+$ [42]. Finally, the CAR-based reactions were supplemented with purified inorganic pyrophosphatase PPA from *E. coli* to prevent activity inhibition by pyrophosphate produced by CAR from ATP [21, 31, 50]. In our previous work, PPA addition was found to be beneficial for the CAR-based transformation of AA to 1,6-hexanediol [42].

Adipaldehyde aminotransferases identified in this work use L-Ala or L-Glu as amine donors and produce pyruvate or α-ketoglutarate as products (Table 1). For Ala-dependent ωTAs, a cyclic cascade reaction has been proposed, which recycles the produced pyruvate back into L-Ala using an alanine dehydrogenase (Ala-DH) in the presence of ammonia [40, 60-63]. The NADH required for activity of Ala-DH can be generated using well established NADH-regenerating systems, e,g. a formate/formate dehydrogenase (FDH) or glucose/glucose dehydrogenase [40]. The feasibility of Ala recycling using Ala-DH has been demonstrated for several ω-transaminases catalyzing asymmetric amination of

different ketones [64-65]. For Glu-dependent ωTAs, the produced α-ketoglutarate can be recycled back into L-Glu using ammonia and a glutamate dehydrogenase (Glu-DH). For transaminase product recycling in our work, we selected the well characterized NADH-dependent Ala-DH BSU3188 from *Bacillus subtilis* (Uniprot Q08352) and NADPH dependent Glu-DH GDH1 from *S. cerevisiae* (P07262) [66-67] (Table S1). For NADPH regeneration, both cyclic cascades were supplemented with the FDH D222Q/H224N double mutant protein, whereas NADH was regenerated using the wild type FDH (Figure 2).

Biotransformation of AA using the wild type CAR+ωTA cascade with cofactor regenerating systems. Without cofactor regenerating systems, the selected ωTAs showed 7 ± 3% conversion of AA to 6-ACA when combined with the wild type CAR MAB4714 in the presence of ATP, NADPH, and amine donor (Figure S5A, data shown for SAV2585). With regenerating systems for ATP, NAD(P)H, and amine donor, these enzymes achieved 40% conversion, whereas the addition of the *E. coli* pyrophosphatase PPA increased 6-ACA production to 90-95% conversion (Figure S5A). Similar conversion rates to 6-ACA were observed with the five tested ωTAs, but only the MAB4714+SAV2585 cascade produced some HMD (1.5-5% conversion) (Figures 3, S5). Therefore, SAV2585 was selected for further studies on AA transformation to 6-ACA and HMD using CARs and ωTAs. The formation of 6-ACA and HMD in reactions with CAR+ωTA cascades was confirmed using LC-MS (Figure S6). The low production of HMD (Figure 3) and low activity of wild type CARs toward 6-ACA observed in our previous work [42] suggest that the presence of a terminal amino group in substrates has an adverse effect on binding/activity of wild type enzymes. Therefore, we proposed that the

reactivity of CARs toward 6-ACA and other aminated substrates could be enhanced using structure-based protein engineering.

Another potential bottleneck in the transformation of AA to HMD might be associated with the low activity of SAV2585 toward aminated intermediates (e.g. 6-aminohexanal). We proposed that putrescine transaminases might exhibit higher aminotransferase activity toward substrates containing terminal amines. A recent report indicated that putrescine TAs represent appealing biocatalysts for biotransformations involving diamines [68]. The *E. coli* putrescine TA PatA belongs to aminotransferase class III (Pfam PF00202) and catalyzes the transfer of an amino group from terminal diamine donor molecules (putrescine, cadaverine) to keto acid acceptors (α-ketoglutarate) [69]. The K_m values for putrescine and α-ketoglutarate were found to be 9.2 mM and 19 mM, respectively [69]. In pyruvate amination reactions, *E. coli* PatA showed a preference for C4-C6 diaminoalkanes as amine donors [68]. Recently, *E. coli* PatA and two other putrescine TAs have been shown to exhibit broad specificity for terminal aliphatic diamines making them attractive biocatalysts. It was also noted that ωTAs, which can accept amines or substrates with an amino group distant from carbonyl, are of special interest for biocatalytic applications [40].

In our work, we observed that purified *E. coli* PatA was also active in HMD deamination with K_m 7.7 mM and k_{cat} 0.4 s^{-1} (k_{cat}/K_m 0.6 × 10^1). As shown in Table 1, PatA exhibited lower activity in the transamination reaction with adipaldehyde as acceptor (with L-glutamate as nitrogen donor), but its K_m for adipaldehyde was almost two orders of magnitude lower (0.1 mM) compared to that for HMD (7.7 mM). Since PatA is likely to be tolerant to the presence of amino groups in substrates, we tested this

enzyme as an additional ωTA in AA transformation using the MAB4714+SAV2585 cascade. Indeed, PatA addition stimulated HMD production both from AA and 6-ACA by the wild type MAB4714 and SAV2585 (Figure 3).

Crystal structure of the CAR A-domain in complex with AMP and succinate. Recent biochemical and structural studies of CARs indicated that A-domains of these enzymes play a major role in substrate recognition [21, 27, 70]. To obtain crystal structures of CAR A-domains for structure-based protein engineering studies, we cloned 16 A-domain fragments from 11 different CARs from our previous work [42] and purified four A-domains for crystallization (including MAB4714 and MCH22995 from *M. chelonae*, 88 % sequence identity, Figure S1). The MCH22995 A-domain (1-641 aa) produced diffracting crystals, and its crystal structure was determined to a resolution of 1.97 Å using molecular replacement and the structure of the *N. iowensis* CAR A-domain (PDB code 5MSD) as the model (Table S2).

The overall structure of the MCH22995 A-domain revealed the prototypic fold of adenylation domains for CARs (*N. iowensis* and *S. rugosus*) and acyl-CoA synthetases from the ANL superfamily (Figure 4A). The MCH22995 A-domain contains two subdomains, an N-terminal subdomain (residues 1-517) and a smaller C-terminal subdomain (residues 518-641) (Figure 4). The structure of the N-terminal subdomain shows a distorted six-stranded antiparallel β-barrel together with two predominantly parallel β-sheets flanked by α-helices, whereas the C-terminal subdomain is made of five β-strands surrounded by five α-helices (Figure 4). The MCH22995 active site is located at the interface between two subdomains as indicated by the bound AMP and succinate, which was presumably carried over through purification from *E. coli* cells (Figure 4).

Most of the MCH22995 residues interacting with AMP and succinate were from the N-terminal subdomain, whereas the conserved Lys621 from the C-terminal domain contributed to binding of the nucleotide phosphate (3.2 Å) and ribofuranose oxygen (3.3 Å) (Figure 5). The adenine base is bound in the *anti* configuration in the deep cleft between the side chains of Tyr422 (3.7 Å) and Tyr510 (4.0 Å), whereas the phosphate moiety was coordinated by the main chain groups of the P-loop (Ser262-Thr267) and Gly423-Thr425 strand (β16-β17, 3.8 Å). The exocyclic N^6-amino group of adenine is hydrogen-bonded to the side chain of conserved Asp420 (2.7 Å), while the side chain of conserved Asp498 forms hydrogen bonds with the 2′ and 3′ ribose hydroxyls (2.5 and 2.7 Å). The ATP-binding channel is adjacent to the acid binding pocket as indicated by the position of the bound succinate (3.1 Å to the AMP phosphate group). The side chain of the conserved His304 is positioned close to the AMP phosphate (3.3 Å) and succinate C4 carboxyl (4.2 Å), likely coordinating both ATP and acid substrate for an adenylation reaction initiated by nucleophilic attack of the acid carboxyl on the ATP α-phosphate.

Substrate binding pocket of MCH22995 and rational protein engineering. The relatively narrow acid binding pocket of MCH22995 is separated from the ATP binding channel by the β15-α15 loop (Ser397-Pro404) and is also defined/bounded by the side chains and main chain groups of α11, β16, and α10-β12 strand (Figure 5). It is lined mostly by hydrophobic amino acids (Trp286, Leu287, Leu305, Ala306, Leu309, and Leu345) and includes several glycine residues (Gly396, Gly398, Gly421, and Gly423) (Figure 5). The side chain of Leu345 is positioned above the succinate C1 carboxyl (3.3-4.3 Å), which is likely close to the position of the adipic acid carboxyl bound in the active site (Figure 5). We hypothesized that binding of 6-ACA in the active site of CARs

(and consequently their activity toward this substrate) can be enhanced by the introduction of residues forming additional interactions with the 6-ACA amino group (e.g. salt bridges or hydrogen bonds). Based on the MCH22995 A-domain structure and CAR sequence alignment (Figure S1), we selected 10 residues from the acid binding pocket of MAB4714 (88 % sequence identity to MCH22995). The targeted residues were Leu342 (Leu345 in MCH22995), as well as several Gly or small residues, which were mutated to Glu, Gln, or hydrophobic residues (Trp, Phe, or Leu) using site-directed mutagenesis.

Overall, 16 MAB4714 mutant proteins were purified, and their reductase activities were compared with the wild type protein using screening with seven different substrates (Figure 5E). With benzoic acid as substrate, most mutant proteins retained significant or wild type activity, except for two Gly420 mutant proteins (G420E and Gly420W), which were also inactive with most of the tested substrates (Figure 5E). In the MCH22995 active site, the homologous Gly423 residue is located at the bottom of the acid-binding site, near the ATP binding channel, suggesting that the introduction of a large side chain at this position will prevent substrate binding.

Reductase activity of the MAB4714 mutant proteins toward AA was more sensitive to mutations with wild type activity observed in three proteins (A303E, L342F, and L342Q) and reduced activity in other mutant proteins (Figure 5E). Notably, enhanced reductase activity against 6-ACA was observed in four mutant proteins including L342E, L342Q, G418E, and G426W, which also retained significant activity toward AA (Figure 5E). However, the L342F mutant protein showed no activity increase toward 6-ACA, suggesting that binding of this substrate in the MAB4714 active site is facilitated by ionic

and/or hydrogen bond interactions (provided by Glu or Gln). The results of substrate screening were confirmed by the analysis of kinetic parameters of purified mutant proteins, which exhibited higher catalytic rates (k_{cat}) and catalytic efficiencies (k_{cat}/K_m) with 6-ACA compared to the wild type protein, while retaining wild type or reduced levels for AA (Table 2). In particular, the L342E protein showed lower K_m and higher k_{cat} with 6-ACA compared to wild type MAB4714, resulting in a 10 times higher catalytic efficiency (Table 2). As presented in Figure 5, the MAB4714 mutations L342E (Leu345 in MCH22995), G418E (G421 in MCH22995), and G426W (Gly429 in MCH22995) can create additional interactions for binding of 6-ACA in the active site. These mutations also greatly enhanced MAB4714 activity toward 7-aminoheptanoic acid and 8-aminooctanoic acid (Figure 5E, Table 2). Specifically, G426W was up to two orders of magnitude more efficient than wild type MAB4714 against these substrates.

***In vitro* biotransformation of 6-ACA and AA using the MAB4714 L342E protein.** Based on kinetic parameters (Table 2), the MAB4714 L342E mutant protein was selected for further studies on AA biotransformation using the CAR+TA cascades. With 6-ACA as substrate, purified L342E and SAV2585 showed up to 50% conversion to HMD compared to 1.5% observed for wild type MAB4714 (Figures 3 and 6). Furthermore, the addition of PatA increased the conversion of 6-ACA to HMD to 70% (Figure 6). As expected, adding wild type MAB4714 to L342E produced no improvement in 6-ACA transformation for reactions containing one or two TAs (due to low activity of wild type protein against 6-ACA). With AA as substrate, the L342E+SAV2585 cascade produced small amounts of both 6-ACA and HMD, and the addition of PatA had a minor positive effect, suggesting that transformation is limited by the low activity of L342E toward AA

(Figure 6). Based on these results, we hypothesized that the conversion of AA to HMD can be improved using a combination of the MAB4714 wild type and L342E proteins, because the wild type enzyme is more active against AA (CAR_1 in Cascade-1), whereas the L342E protein is more efficient toward 6-ACA (CAR_2 in Cascade-2). Similarly, the inclusion of PatA might also be beneficial, since this enzyme appears to improve HMD formation from 6-ACA (TA_2 Cascade-2) (Figures 3 and 6). Accordingly, when both the wild type and L342E proteins were used in combination with one or two TAs for AA transformation, the reactions resulted in 30% conversion to HMD (and 60-70% to 6-ACA) representing a two times improvement compared to the wild type MAB4714 alone (Figures 3 and 6).

CONCLUSIONS

The biocatalytic transformation of terminal diacids (adipic acid) to terminal diamines (HMD) using CARs and ωTAs represents a formidable challenge due to the necessity to accommodate substrates with different terminal groups (carboxyl, carbonyl, amine) in substrate binding sites. Here we demonstrated that purified wild type MAB4714 and SAV2585 catalyze efficient transformation of AA to 6-ACA with up to 95% conversion but showed low activity in the second round of reduction/amination reactions (6-ACA → HMD). Using structure-based protein engineering, we generated three mutant variants of MAB4714 (L342E, G418E, G426W) with enhanced activity toward 6-ACA, as well as against 7-aminoheptanoic acid and 8-aminooctanoic acid. In combination with SAV2585 and putrescine transaminase PatA, the L342E variant showed up to 75% conversion of 6-ACA to HMD but exhibited low activity against AA (the Cascade-1). Therefore, for one-

pot transformation of AA to HMD (via 6-ACA, Cascades 1 and 2, Figure 1), the wild type MAB4714 and SAV2585 were supplemented with the MAB4714 L342E variant and putrescine transaminase PatA, resulting in a complete conversion of AA to HMD (30%) and 6-ACA (70%). We propose that HMD production from AA can be further improved by combining the identified beneficial mutations of MAB4714 (L342E, G418E, and G426W) and potentially via protein engineering of TAs. Thus, our study provided insights into the molecular mechanisms of substrate selectivity of CARs and illustrated the suitability of CARs and ωTAs for two rounds of substrate reduction/amination in one-pot cascade systems.

ASSOCIATED CONTENT

Supporting Information

The Supporting Information is available free of charge on the ACS Publications website at DOI:

Figures S1 – S6, Tables S1 – S3 (PDF)

Accession Codes

The structure of the MCH22995 A-domain in complex with AMP and succinate is deposited to the Protein Data Bank with PDB ID 6OZ1.

Notes

The authors declare no competing financial interests.

ACKNOWLEDGMENTS

The authors thank all members of the BioZone Centre for Applied Science and Bioengineering and Biozone MS-facility for help in conducting the experiments. This work was supported by the Natural Sciences and Engineering Research Council (NSERC) Strategic Network grant IBN, Ontario Research Fund (ORF Research Excellence) grant BioCeB (Biochemicals from Cellulosic Biomass), and a grant from Genome Canada, Genomics Applied Partnership Program (GAPP).

REFERENCES

1. Schaffer, S., and Haas, T., Biocatalytic and fermentative production of a,omega-bifunctional polymer precursors. *Org. Process Res. Dev.* **2014,** *18*, 752-766.
2. Chae, T. U.; Ahn, J. H.; Ko, Y. S.; Kim, J. W.; Lee, J. A.; Lee, E. H.; Lee, S. Y., Metabolic engineering for the production of dicarboxylic acids and diamines. *Metab Eng* **2019**, (published online, PMID 30905694).
3. Polen, T.; Spelberg, M.; Bott, M., Toward biotechnological production of adipic acid and precursors from biorenewables. *J Biotechnol* **2013,** *167*, 75-84.
4. Lee, S. Y., Kim, H.U., Chae, T.U., Cho, J.S., Kim, J.W., Shin, J.H., Kim, D.I., Ko, Y.-S., Jang, W.D., and Jang, Y.-S., A comprehensive metabolic map for production of bio-based chemicals. *Nature Catalysis* **2019,** *2*, 18-33.
5. van de Vyver, S., and Roman-Leshkov, Y., Emerging catalytic processes for the production of adipic acid. *Catal. Sci. Technol.* **2013,** *3*, 1465-1479.
6. Belussi, G., and Perego, C., Industrial catalytic aspects of the synthesis of monomers for nylon production. *CATTECH* **2000,** *4*, 4-16.
7. Mormul, J., Breitenfeld, J., Trapp, O., Paciello, R., Schaub, T., and Hofmann, P., Synthesis of adipic axcid, 1,6-hexanediamine, and 1,6-hexanediol via double-n-selective hydroformylation of 1,3-bitadiene. *ACS Catalysis* **2016,** *6*, 2802-2810.
8. Beardslee, T., and Picataggio, S., Bio-based adipic acid from renewable oils. *Lipid Technol.* **2012,** *24*, 223-225.
9. Yu, J. L.; Xia, X. X.; Zhong, J. J.; Qian, Z. G., Direct biosynthesis of adipic acid from a synthetic pathway in recombinant *Escherichia coli*. *Biotechnol Bioeng* **2014,** *111*, 2580-6.
10. Cheong, S.; Clomburg, J. M.; Gonzalez, R., Energy- and carbon-efficient synthesis of functionalized small molecules in bacteria using non-decarboxylative Claisen condensation reactions. *Nat Biotechnol* **2016,** *34*, 556-61.
11. Deng, Y.; Mao, Y., Production of adipic acid by the native-occurring pathway in *Thermobifida fusca* B6. *J Appl Microbiol* **2015,** *119*, 1057-63.
12. Zhao, M.; Huang, D.; Zhang, X.; Koffas, M. A. G.; Zhou, J.; Deng, Y., Metabolic engineering of *Escherichia coli* for producing adipic acid through the reverse adipate-degradation pathway. *Metab Eng* **2018,** *47*, 254-262.

13. Clomburg, J. M.; Blankschien, M. D.; Vick, J. E.; Chou, A.; Kim, S.; Gonzalez, R., Integrated engineering of beta-oxidation reversal and omega-oxidation pathways for the synthesis of medium chain omega-functionalized carboxylic acids. *Metab Eng* **2015,** *28*, 202-212.
14. Joo, J. C.; Khusnutdinova, A. N.; Flick, R.; Kim, T.; Bornscheuer, U. T.; Yakunin, A. F.; Mahadevan, R., Alkene hydrogenation activity of enoate reductases for an environmentally benign biosynthesis of adipic acid. *Chem Sci* **2017,** *8*, 1406-1413.
15. Raj, K.; Partow, S.; Correia, K.; Khusnutdinova, A. N.; Yakunin, A. F.; Mahadevan, R., Biocatalytic production of adipic acid from glucose using engineered *Saccharomyces cerevisiae*. *Metab Eng Commun* **2018,** *6*, 28-32.
16. Sun, J.; Raza, M.; Sun, X.; Yuan, Q., Biosynthesis of adipic acid via microaerobic hydrogenation of cis,cis-muconic acid by oxygen-sensitive enoate reductase. *J Biotechnol* **2018,** *280*, 49-54.
17. Hagen, A.; Poust, S.; Rond, T.; Fortman, J. L.; Katz, L.; Petzold, C. J.; Keasling, J. D., Engineering a Polyketide Synthase for In Vitro Production of Adipic Acid. *ACS Synth Biol* **2016,** *5*, 21-7.
18. Turk, S. C.; Kloosterman, W. P.; Ninaber, D. K.; Kolen, K. P.; Knutova, J.; Suir, E.; Schurmann, M.; Raemakers-Franken, P. C.; Muller, M.; de Wildeman, S. M.; Raamsdonk, L. M.; van der Pol, R.; Wu, L.; Temudo, M. F.; van der Hoeven, R. A.; Akeroyd, M.; van der Stoel, R. E.; Noorman, H. J.; Bovenberg, R. A.; Trefzer, A. C., Metabolic Engineering toward Sustainable Production of Nylon-6. *ACS Synth Biol* **2016,** *5*, 65-73.
19. Akhtar, M. K.; Turner, N. J.; Jones, P. R., Carboxylic acid reductase is a versatile enzyme for the conversion of fatty acids into fuels and chemical commodities. *Proc Natl Acad Sci U S A* **2013,** *110*, 87-92.
20. Sheppard, M. J.; Kunjapur, A. M.; Prather, K. L. J., Modular and selective biosynthesis of gasoline-range alkanes. *Metab Eng* **2016,** *33*, 28-40.
21. Finnigan, W.; Thomas, A.; Cromar, H.; Gough, B.; Snajdrova, R.; Adams, J. P.; Littlechild, J. A.; Harmer, N. J., Characterization of Carboxylic Acid Reductases as Enzymes in the Toolbox for Synthetic Chemistry. *ChemCatChem* **2017,** *9*, 1005-1017.
22. Napora-Wijata, K.; Strohmeier, G. A.; Winkler, M., Biocatalytic reduction of carboxylic acids. *Biotechnol J* **2014,** *9*, 822-43.
23. Li, T.; Rosazza, J. P., Purification, characterization, and properties of an aryl aldehyde oxidoreductase from *Nocardia* sp. strain NRRL 5646. *J Bacteriol* **1997,** *179*, 3482-7.
24. Li, T.; Rosazza, J. P., NMR identification of an acyl-adenylate intermediate in the aryl-aldehyde oxidoreductase catalyzed reaction. *J Biol Chem* **1998,** *273*, 34230-3.
25. Venkitasubramanian, P.; Daniels, L.; Rosazza, J. P., Reduction of carboxylic acids by *Nocardia* aldehyde oxidoreductase requires a phosphopantetheinylated enzyme. *J Biol Chem* **2007,** *282*, 478-85.
26. He, A.; Li, T.; Daniels, L.; Fotheringham, I.; Rosazza, J. P., *Nocardia* sp. carboxylic acid reductase: cloning, expression, and characterization of a new aldehyde oxidoreductase family. *Appl Environ Microbiol* **2004,** *70*, 1874-81.
27. Gahloth, D.; Dunstan, M. S.; Quaglia, D.; Klumbys, E.; Lockhart-Cairns, M. P.; Hill, A. M.; Derrington, S. R.; Scrutton, N. S.; Turner, N. J.; Leys, D., Structures of carboxylic acid reductase reveal domain dynamics underlying catalysis. *Nat Chem Biol* **2017,** *13*, 975-981.
28. Venkitasubramanian, P.; Daniels, L.; Das, S.; Lamm, A. S.; Rosazza, J. P., Aldehyde oxidoreductase as a biocatalyst: Reductions of vanillic acid. *Enzyme Microb Technol* **2008,** *42*, 130-7.
29. Sheppard, M. J.; Kunjapur, A. M.; Wenck, S. J.; Prather, K. L., Retro-biosynthetic screening of a modular pathway design achieves selective route for microbial synthesis of 4-methyl-pentanol. *Nat Commun* **2014,** *5*, 5031.

30. Kunjapur, A. M.; Tarasova, Y.; Prather, K. L., Synthesis and accumulation of aromatic aldehydes in an engineered strain of *Escherichia coli*. *J Am Chem Soc* **2014,** *136*, 11644-54.
31. Schwendenwein, D.; Fiume, G.; Weber, H.; Rudroff, F.; Winkler, M., Selective Enzymatic Transformation to Aldehydes in vivo by Fungal Carboxylate Reductase from *Neurospora crassa*. *Adv Synth Catal* **2016,** *358*, 3414-3421.
32. Kallio, P.; Pasztor, A.; Thiel, K.; Akhtar, M. K.; Jones, P. R., An engineered pathway for the biosynthesis of renewable propane. *Nat Commun* **2014,** *5*, 4731.
33. Cosgrove, S. C.; Brzezniak, A.; France, S. P.; Ramsden, J. I.; Mangas-Sanchez, J.; Montgomery, S. L.; Heath, R. S.; Turner, N. J., Imine Reductases, Reductive Aminases, and Amine Oxidases for the Synthesis of Chiral Amines: Discovery, Characterization, and Synthetic Applications. *Methods Enzymol* **2018,** *608*, 131-149.
34. France, S. P., Hussain, S., Hill, A.M., Hepworth, L.J., Howard, R.M., Mulholland, K.R., Flitsch, S.L., and Turner, N.J., One-pot cascade synthesis of mono- and disubstituted piperidines and pyrrolidines using carboxylic acid reductase, omega-transaminase, and imine reductase biocatalysts. *ACS Catalysis* **2016,** *6*, 3753-3759.
35. Ramsden, J. I.; Heath, R. S.; Derrington, S. R.; Montgomery, S. L.; Mangas-Sanchez, J.; Mulholland, K. R.; Turner, N. J., Biocatalytic N-Alkylation of Amines Using Either Primary Alcohols or Carboxylic Acids via Reductive Aminase Cascades. *J Am Chem Soc* **2019,** *141*, 1201-1206.
36. Derrington, S. R., Turner, N.J., and France, S.P., Carboxylic acid reductases (CARs): an industrial perspective. *J. Biotechnol.* **2019,** *304*, 78-88.
37. Percudani, R.; Peracchi, A., The B6 database: a tool for the description and classification of vitamin B6-dependent enzymatic activities and of the corresponding protein families. *BMC Bioinformatics* **2009,** *10*, 273.
38. Steffen-Munsberg, F.; Vickers, C.; Kohls, H.; Land, H.; Mallin, H.; Nobili, A.; Skalden, L.; van den Bergh, T.; Joosten, H. J.; Berglund, P.; Hohne, M.; Bornscheuer, U. T., Bioinformatic analysis of a PLP-dependent enzyme superfamily suitable for biocatalytic applications. *Biotechnol Adv* **2015,** *33*, 566-604.
39. Slabu, I., Galman, J.L., Lloyd, R.C., and Turner, N.J., Discovery, engineering, and synthetic applications of transaminase biocatalysts. *ACS Catalysis* **2017,** *7*, 8263-8284.
40. Guo, F., and Berglund, P., Transaminase biocatalysis: optimization and application. *Green Chem.* **2017,** *19*, 333-360.
41. Patil, M. D., Grogan, G., Bommarius, A., and Yun, H., Recent advances in omega-transaminase-mediated biocatalysis for the enantioselective synthesis of chiral amines. *Catalysts* **2018,** *8*, 254.
42. Khusnutdinova, A. N.; Flick, R.; Popovic, A.; Brown, G.; Tchigvintsev, A.; Nocek, B.; Correia, K.; Joo, J. C.; Mahadevan, R.; Yakunin, A. F., Exploring Bacterial Carboxylate Reductases for the Reduction of Bifunctional Carboxylic Acids. *Biotechnol J* **2017,** *12* (11).
43. Kuznetsova, E.; Proudfoot, M.; Gonzalez, C. F.; Brown, G.; Omelchenko, M. V.; Borozan, I.; Carmel, L.; Wolf, Y. I.; Mori, H.; Savchenko, A. V.; Arrowsmith, C. H.; Koonin, E. V.; Edwards, A. M.; Yakunin, A. F., Genome-wide analysis of substrate specificities of the *Escherichia coli* haloacid dehalogenase-like phosphatase family. *J Biol Chem* **2006,** *281*, 36149-61.
44. Kitagawa, M.; Ara, T.; Arifuzzaman, M.; Ioka-Nakamichi, T.; Inamoto, E.; Toyonaga, H.; Mori, H., Complete set of ORF clones of *Escherichia coli* ASKA library (a complete set of E. coli K-12 ORF archive): unique resources for biological research. *DNA Res* **2005,** *12*, 291-9.
45. Beloglazova, N.; Lemak, S.; Flick, R.; Yakunin, A. F., Analysis of nuclease activity of Cas1 proteins against complex DNA substrates. *Methods Mol Biol* **2015,** *1311*, 251-64.
46. Katoh, K.; Rozewicki, J.; Yamada, K. D., MAFFT online service: multiple sequence alignment, interactive sequence choice and visualization. *Brief Bioinform* **2019,** *20*, 1160-6.

47. Gille, C.; Fahling, M.; Weyand, B.; Wieland, T.; Gille, A., Alignment-Annotator web server: rendering and annotating sequence alignments. *Nucleic Acids Res* **2014,** *42*, W3-6.
48. Wilding, M.; Walsh, E. F.; Dorrian, S. J.; Scott, C., Identification of novel transaminases from a 12-aminododecanoic acid-metabolizing *Pseudomonas* strain. *Microb Biotechnol* **2015,** *8*, 665-72.
49. Hu, H.; Liang, Y.; Li, S.; Guo, Q.; Wu, C., A Modified o-Phthalaldehyde Fluorometric Analytical Method for Ultratrace Ammonium in Natural Waters Using EDTA-NaOH as Buffer. *J Anal Methods Chem* **2014,** *2014*, 728068.
50. Kunjapur, A. M., Cervantes, B., and Prather, K.L.J., Coupling carboxylic acid reductase to inorganic pyrophosphatase enhances cell-free in vitro aldehyde biosynthesis. *Biochem. Eng. J.* **2016,** *109*, 19-27.
51. Minor, W.; Cymborowski, M.; Otwinowski, Z.; Chruszcz, M., HKL-3000: the integration of data reduction and structure solution--from diffraction images to an initial model in minutes. *Acta Crystallogr D Biol Crystallogr* **2006,** *62*, 859-66.
52. Adams, P. D.; Afonine, P. V.; Bunkoczi, G.; Chen, V. B.; Davis, I. W.; Echols, N.; Headd, J. J.; Hung, L. W.; Kapral, G. J.; Grosse-Kunstleve, R. W.; McCoy, A. J.; Moriarty, N. W.; Oeffner, R.; Read, R. J.; Richardson, D. C.; Richardson, J. S.; Terwilliger, T. C.; Zwart, P. H., PHENIX: a comprehensive Python-based system for macromolecular structure solution. *Acta Crystallogr D Biol Crystallogr* **2010,** *66*, 213-21.
53. Kelley, L. A.; Mezulis, S.; Yates, C. M.; Wass, M. N.; Sternberg, M. J., The Phyre2 web portal for protein modeling, prediction and analysis. *Nat Protoc* **2015,** *10*, 845-58.
54. Emsley, P.; Lohkamp, B.; Scott, W. G.; Cowtan, K., Features and development of Coot. *Acta Crystallogr D Biol Crystallogr* **2010,** *66*, 486-501.
55. Hummel, W.; Groger, H., Strategies for regeneration of nicotinamide coenzymes emphasizing self-sufficient closed-loop recycling systems. *J Biotechnol* **2014,** *191*, 22-31.
56. Vrtis, J. M.; White, A. K.; Metcalf, W. W.; van der Donk, W. A., Phosphite dehydrogenase: a versatile cofactor-regeneration enzyme. *Angew Chem Int Ed Engl* **2002,** *41*, 3257-9.
57. Wang, X., Saba, T., Yiu, H.H.P., Howe, R.F., Anderson, J.A., and Shi, J., Cofactor NAD(P)H regeneration inspired by heterologous pathways. *Chem* **2017,** *2*, 621-654.
58. Nocek, B. P., Khusnutdinova, A.N., Ruszkowski, M., Flick, R., Burda, M., Batyrova, K., Brown, G., Mucha, A., Joachimiak, A., Berlicki, L., and Yakunin A.F., Structural insights into substrate selectivity and activity of bacterial polyphosphate kinases. *ACS Catalysis* **2018,** *8*, 10746-10760.
59. Tishkov, V. I.; Galkin, A. G.; Marchenko, G. N.; Egorova, O. A.; Sheluho, D. V.; Kulakova, L. B.; Dementieva, L. A.; Egorov, A. M., Catalytic properties and stability of a *Pseudomonas* sp.101 formate dehydrogenase mutants containing Cys-255-Ser and Cys-255-Met replacements. *Biochem Biophys Res Commun* **1993,** *192*, 976-81.
60. Simon, R. C., Richter, N., Busto, E., and Kroutil, W., Recent developments of cascade reactions involving transaminases *ACS Catalysis* **2014,** *4*, 129-143.
61. Galkin, A., Kulakova, L., Yamamoto, H., Tanizawa, K., Tanaka, H., Esaki, N., and Soda, K., Conversion of alpha-keto acids to D-amino acids by coupling of four enzyme reactions. *J. Ferment. Bioeng.* **1997,** *83*, 299-300.
62. Fuchs, M.; Farnberger, J. E.; Kroutil, W., The Industrial Age of Biocatalytic Transamination. *European J Org Chem* **2015,** *2015*, 6965-6982.
63. Richter, N., Farnberger, J.E., Pressnitz, D., Lechner, H., Zepeck, F., and Kroutil, W., A system for transaminase mediated (R)-amination using L-alanine as an amine donor. *Green Chem.* **2015,** *17*, 2952-2958.

64. Mutti, F. G., Fuchs, C.S., Pressnitz, D., Sattler, J.H., and Kroutil, W., Stereoselectivity of four (R)-selective transaminases for the asymmetic amination of ketones. *Adv Synth Catal* **2011,** *353*, 3227-3233.
65. Pressnitz, D., Fuchs, C.S., Sattler, J.H., Knaus, T., Macheroux, P., Mutti, F.G., and Kroutil, W., Asymmetric amination of tetralone and chromanone derivatives employing transaminases. *ACS Catalysis* **2013,** *3*, 555-559.
66. Lerchner, A.; Jarasch, A.; Skerra, A., Engineering of alanine dehydrogenase from *Bacillus subtilis* for novel cofactor specificity. *Biotechnol Appl Biochem* **2016,** *63*, 616-624.
67. Moye, W. S.; Amuro, N.; Rao, J. K.; Zalkin, H., Nucleotide sequence of yeast GDH1 encoding nicotinamide adenine dinucleotide phosphate-dependent glutamate dehydrogenase. *J Biol Chem* **1985,** *260*, 8502-8.
68. Slabu, I., Galman, J.L., Weise, N.J., Lloyd, R.C., and Turner, N.J., Putrescine transaminases for the synthesis of saturated nitrogen heterocycles from polyamines. *ChemCatChem* **2016,** *8*, 1038-1042.
69. Samsonova, N. N.; Smirnov, S. V.; Altman, I. B.; Ptitsyn, L. R., Molecular cloning and characterization of *Escherichia coli* K12 ygjG gene. *BMC Microbiol* **2003,** *3*, 2.
70. Stolterfoht, H.; Steinkellner, G.; Schwendenwein, D.; Pavkov-Keller, T.; Gruber, K.; Winkler, M., Identification of Key Residues for Enzymatic Carboxylate Reduction. *Front Microbiol* **2018,** *9*, 250.
71. Weinstein, J. N.; Myers, T. G.; O'Connor, P. M.; Friend, S. H.; Fornace, A. J., Jr.; Kohn, K. W.; Fojo, T.; Bates, S. E.; Rubinstein, L. V.; Anderson, N. L.; Buolamwini, J. K.; van Osdol, W. W.; Monks, A. P.; Scudiero, D. A.; Sausville, E. A.; Zaharevitz, D. W.; Bunow, B.; Viswanadhan, V. N.; Johnson, G. S.; Wittes, R. E.; Paull, K. D., An information-intensive approach to the molecular pharmacology of cancer. *Science* **1997,** *275*, 343-9.

Table 1. Kinetic parameters of purified ωTAs with adipaldehyde as substrate.

Transaminase (aminodonor)	K_m, mM	k_{cat}, s^{-1}	k_{cat}/K_m, $M^{-1}s^{-1}$
1. GabT (Glu)	0.57 ± 0.07	1.19 ± 0.06	$1.98 \pm 0.21 \times 10^3$
2. PatA (Glu)	0.10 ± 0.02	0.06 ± 0.01	$0.70 \pm 0.20 \times 10^3$
3. RHA07987 (Ala)	0.99 ± 0.28	0.47 ± 0.05	$0.45 \pm 0.11 \times 10^3$
4. SAV2585 (Glu)	0.29 ± 0.03	0.46 ± 0.10	$1.55 \pm 0.69 \times 10^3$
5. SM5064 (Ala)	0.09 ± 0.03	0.44 ± 0.04	$5.41 \pm 0.89 \times 10^3$
6. SPO3471 (Ala)	1.27 ± 0.10	0.71 ± 0.13	$0.66 \pm 0.20 \times 10^3$

Table 2. Kinetic parameters of purified wild type and mutant MAB4714 proteins with different substrates.

Substrates	**Proteins**	K_m, **mM**	k_{cat}, s^{-1}	k_{cat}/K_m, $M^{-1}\ s^{-1}$
benzoic acid	wild type	0.6 ± 0.1	8.60 ± 0.15	$1.46 \pm 0.04 \times 10^4$
	L342E	4.3 ± 0.6	3.04 ± 0.25	$6.49 \pm 1.16 \times 10^2$
	G418E	2.3 ± 0.5	5.04 ± 0.50	$1.97 \pm 0.44 \times 10^3$
	G426W	1.0 ± 0.2	3.48 ± 0.43	$3.05 \pm 0.86 \times 10^3$
adipic acid	wild type	23.5 ± 2.8	2.16 ± 0.07	$8.89 \pm 0.60 \times 10^1$
	L342E	56.6 ± 5.0	2.72 ± 0.09	$4.65 \pm 0.31 \times 10^1$
	G418E	18.7 ± 2.5	4.25 ± 0.26	$2.03 \pm 0.28 \times 10^2$
	G426W	24.4 ± 2.8	1.94 ± 0.07	$7.66 \pm 0.58 \times 10^1$
6-ACA	wild type	183.3 ± 28.7	0.77 ± 0.07	3.83 ± 0.76
	L342E	70.1 ± 14.5	2.60 ± 0.22	$3.50 \pm 0.63 \times 10^1$
	G418E	490.9 ± 44.2	3.26 ± 0.12	6.41 ± 0.48
	G426W	189.1 ± 42.7	2.31 ± 0.31	$1.06 \pm 0.33 \times 10^1$
7-AHA[a]	wild type	315.6 ± 58.2	0.44 ± 0.04	1.27 ± 0.25
	L342E	10.2 ± 1.1	0.64 ± 0.02	$6.08 \pm 0.39 \times 10^1$
	G418E	78.3 ± 11.9	1.02 ± 0.07	$1.21 \pm 0.18 \times 10^1$
	G426W	38.9 ± 6.1	5.12 ± 0.29	$1.24 \pm 0.15 \times 10^2$
8-AOA[b]	wild type	34.0 ± 2.5	2.62 ± 0.02	$7.65 \pm 0.11 \times 10^1$
	L342E	6.6 ± 1.0	5.28 ± 0.33	$7.50 \pm 1.00 \times 10^2$
	G418E	53.9 ± 6.0	2.57 ± 0.09	$4.60 \pm 0.34 \times 10^1$
	G426W	40.4 ± 6.6	12.3 ± 0.72	$2.87 \pm 0.35 \times 10^2$

[a] 7-AHA, 7-aminoheptanoic acid.

[b] 8-AOA, 8-aminooctanoic acid.

Figure 1

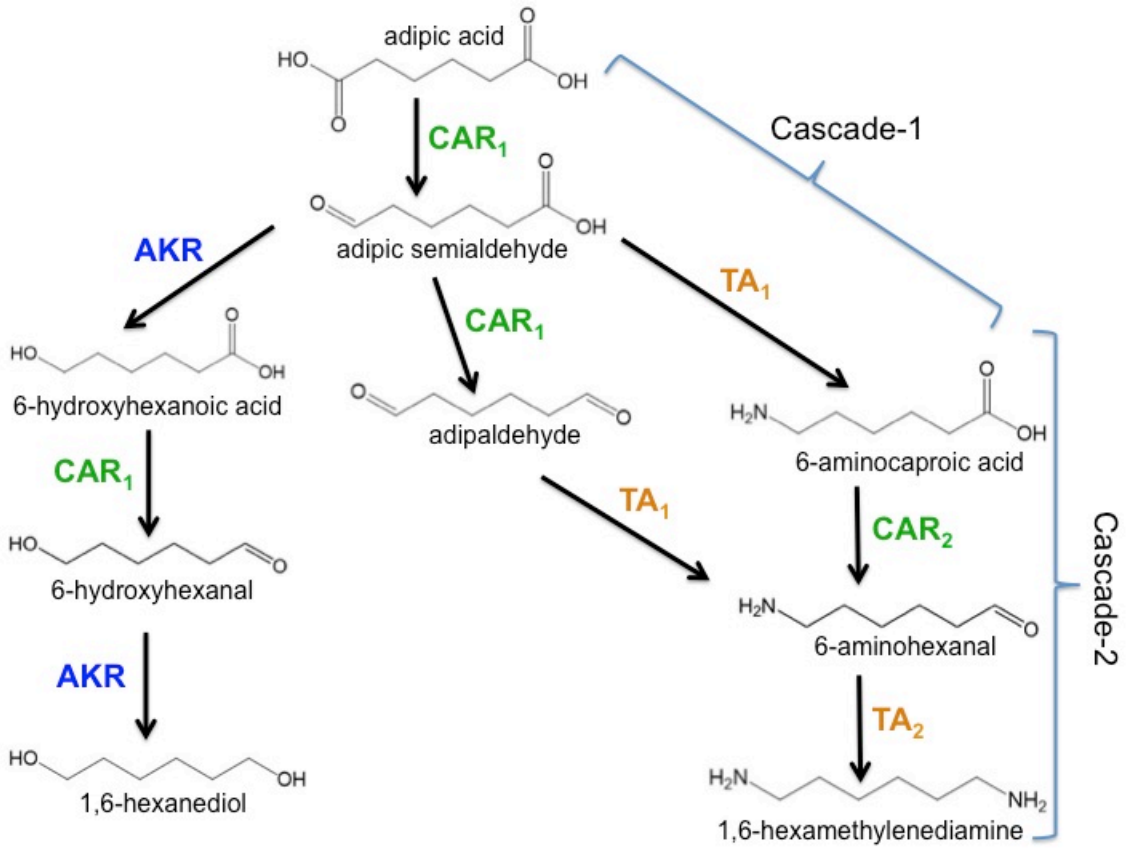

Figure 1. Biochemical reactions for the bioconversion of adipic acid using CARs and other enzymes. Biotransformations of adipic acid to 6-hydroxyhexanoic acid and 1,6-hexanediol using CARs and aldo-keto reductases (AKR) have been demonstrated in our previous work [42]. In this study, we propose using CARs and transaminases (TA) for the bioconversion of adipic acid (AA) to 6-aminocaproic acid (6-ACA) (Cascade-1) and then to 1,6-hexamethylenediamine (HMD) (Cascade-2). CAR_1 indicates wild type CAR, CAR_2 – engineered CAR, and TA_1/TA_2 – different ω-transaminases (ωTAs).

Figure 2

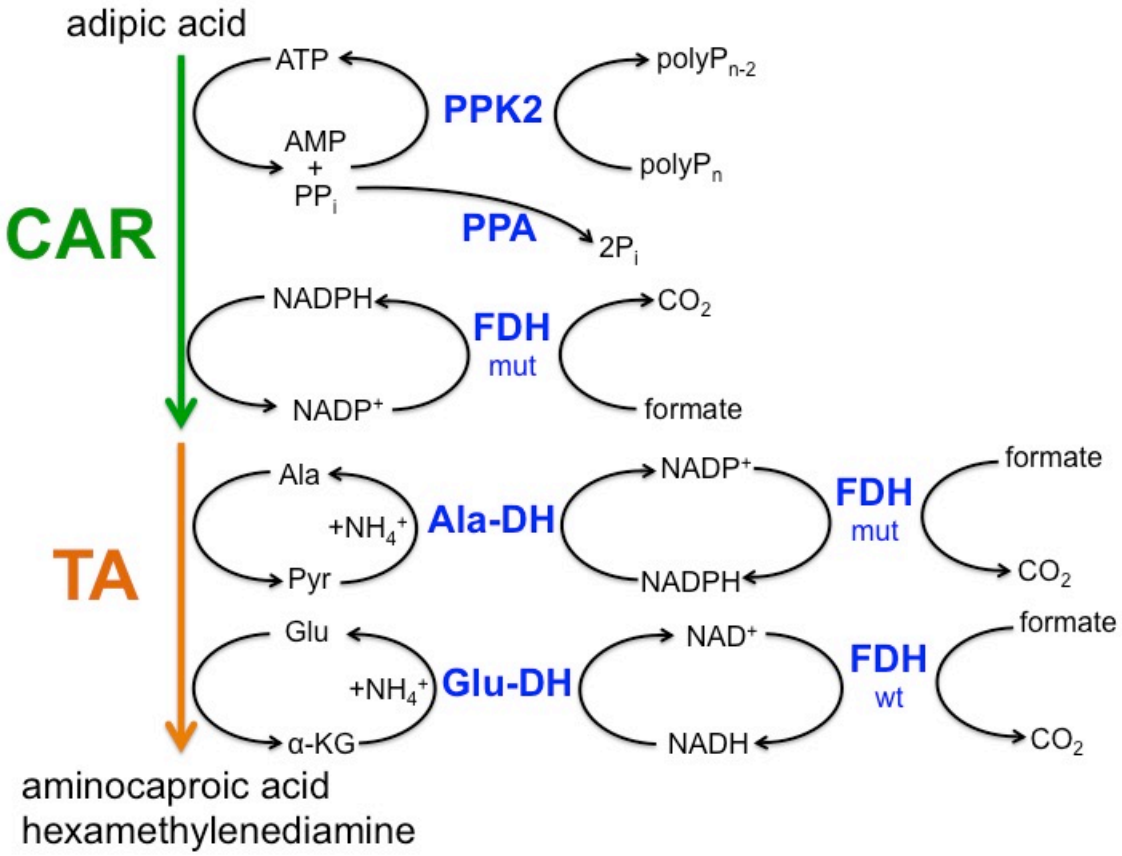

Figure 2. Cofactor regenerating systems used in this work for *in vitro* bioconversion of adipic acid (AA) to 6-aminocaproic acid (6-ACA) and 1,6-hexamethylenediamine (HMD) using CARs and ωTAs. Ala-DH, alanine dehydrogenase; FDHwt, wild type formate dehydrogenase; FDH mutant, D222Q/H224N mutant formate dehydrogenase; Glu-DH, glutamate dehydrogenase; polyP, polyphosphate; PPK2, polyphosphate kinase family 2; PPA, pyrophosphatase. See Materials and Methods for experimental details.

Figure 3

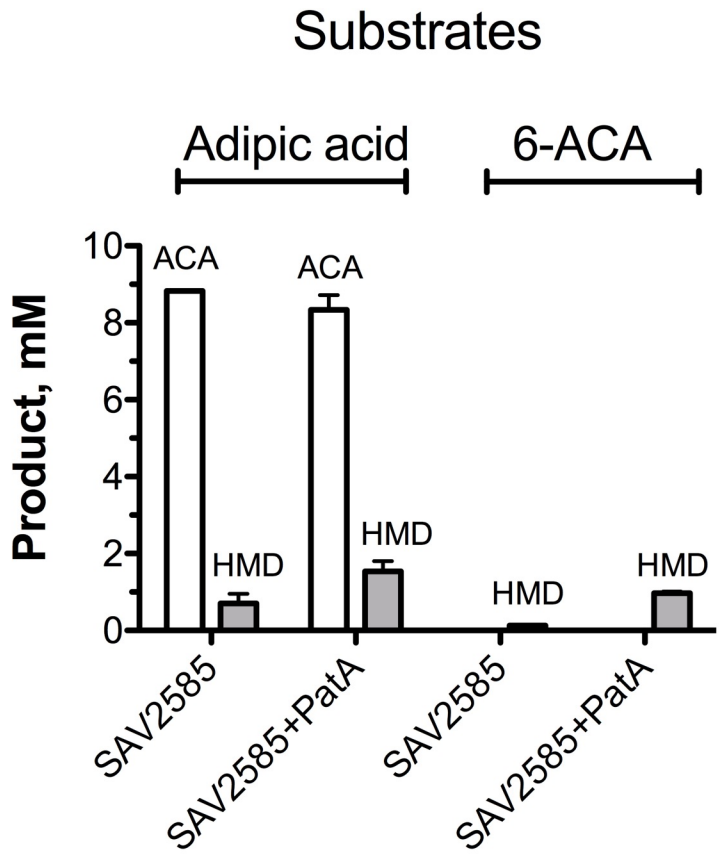

Figure 3. *In vitro* biotransformation of adipic acid (AA) and 6-aminocaproic acid (6-ACA) using wild type MAB4714 and ωTAs. Reaction mixtures contained 10 mM substrate (AA or 6-ACA), regenerating systems (see Materials and Methods), 80 μg of MAB4714, and 20 μg of ωTA (SAV2585 or PatA).

Figure 4

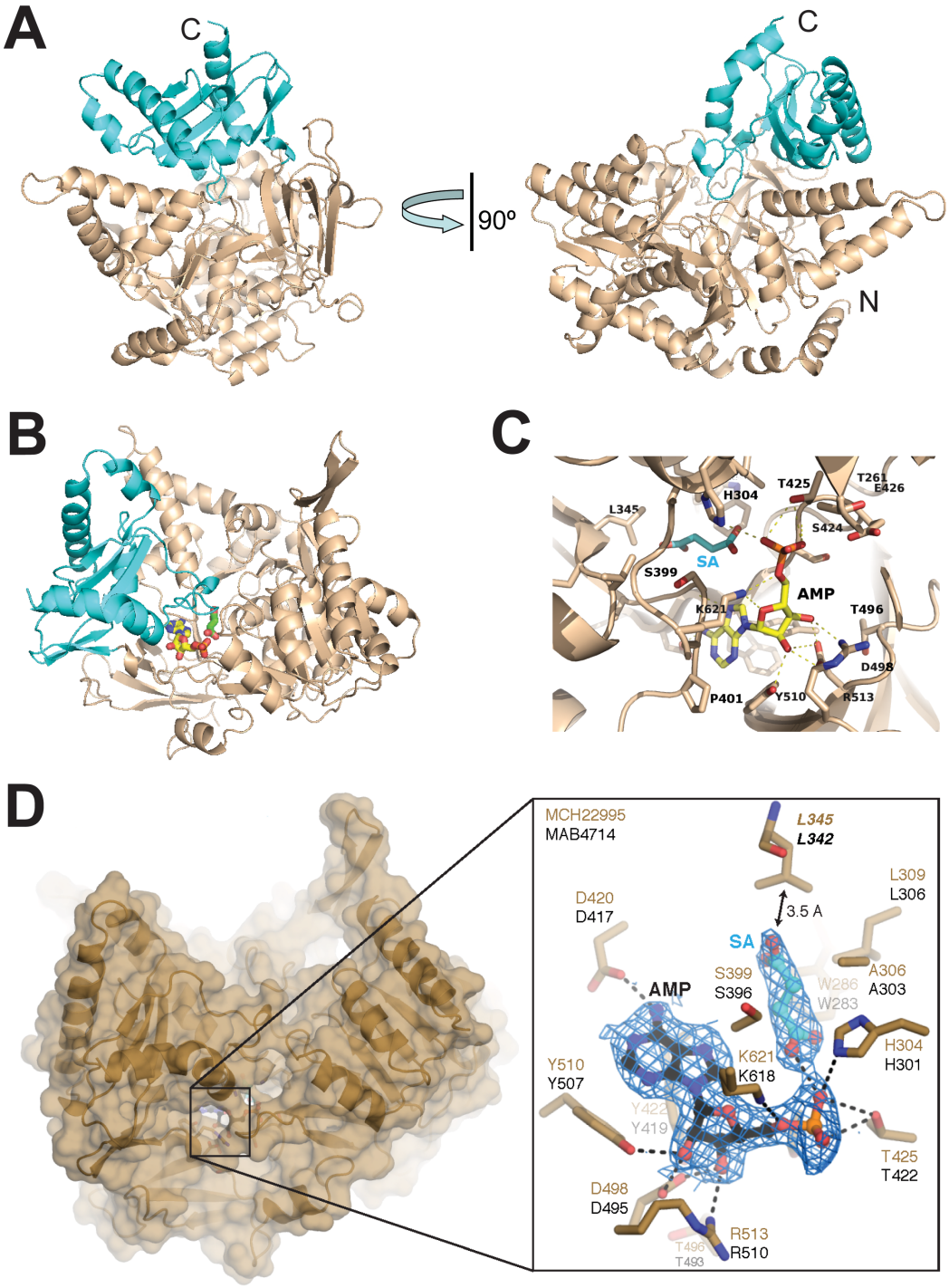

Figure 4. Crystal structure of the MCH22995 A-domain in complex with AMP and succinic acid. (A), Overall fold of the A-domain (1-641 aa) showing two views related by 90° rotation. The protein is shown as a ribbon diagram with the core sub-domain colored wheat and C-terminal sub-domain colored cyan. The protein termini are designated as N and C. (B), The A-domain structure showing the position of two ligands bound in the

active site. Protein ribbon diagram is colored as in A, whereas the ligands are shown as sticks with carbons colored yellow (AMP) and cyan (succinate). (C) Close-up view of the A domain active site with bound AMP and succinate. The ligand molecules are shown as stick models with yellow (AMP) or cyan (succinic acid) carbons, whereas side chains of the active site are shown as sticks with brown carbons. (D), Structural superimposition of the A-domains of MCH22995 (PDB code 6OZ1) and MAB4714 showing the equivalent residues in their active sites (generated using Phyre2). The right panel presents a zoomed in image of the substrate binding pocket. Electron densities shown for AMP and succinate are a simulated annealing *Fo-Fc* map contoured at 2.0 σ, generated with coordinates for AMP and succinate omitted. Dashed lines indicate hydrogen bonds or electrostatic interactions. Residues are labeled in brown for MCH22995 and black for MAB4714. L345/L342 (which is targeted for mutagenesis) is italicized, and its distance from succinate is indicated.

Figure 5

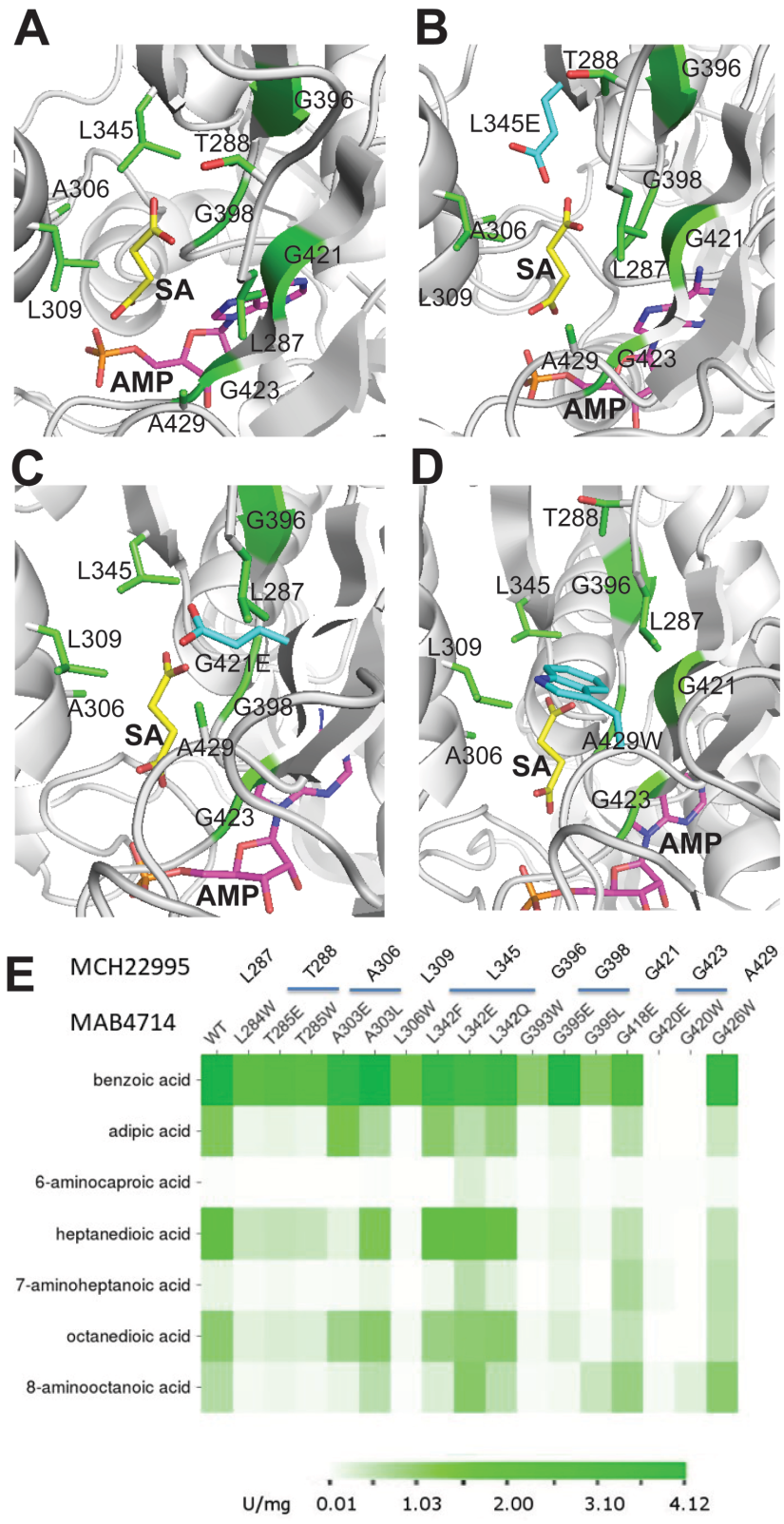
A
L345
T288
G396
A306
G398
G421
SA
L309
L287
AMP
G423
A429
B
T288
G396
L345E
G398
A306
G421
SA
L287
L309
A429
G423
AMP
C
G396
L345
L287
L309
G421E
A306
G398
SA
A429
G423
AMP
D
T288
L345
G396
L287
L309
G421
A429W
A306
SA
G423
AMP
E
MCH22995
MAB4714
L287
T288
A306
L309
L345
G396
G398
G421
G423
A429
WT
L284W
T285E
T285W
A303E
A303L
L306W
L342F
L342E
L342Q
G393W
G395E
G395L
G418E
G420E
G420W
G426W
benzoic acid
adipic acid
6-aminocaproic acid
heptanedioic acid
7-aminoheptanoic acid
octanedioic acid
8-aminooctanoic acid
U/mg
0.01
1.03
2.00
3.10
4.12

Figure 5. Carboxylate binding pocket of CAR (MCH22995) and substrate profiles of purified mutant proteins (MAB4714). A close-up view of substrate binding pockets: (A), wild type protein; (B, C, D), mutant proteins with Leu345 mutated to Glu (B), or Gly421 mutated to Glu (C), or Ala429 mutated to Trp (D) (energy minimized models generated using YASARA). Protein ribbon diagrams are colored gray with side chains shown as sticks with green (wild type) or cyan (mutants) carbons. The bound succinic acid (SA) and AMP are shown as stick models with yellow (SA) or magenta (AMP) carbons. (D), Carboxylate reductase activities of purified MAB4714 mutant proteins: substrate profiles. The corresponding MCH22995 residues presented in panels A-D are shown above the mutated residues of MAB4714. The heat map represents CAR activities of purified proteins (U/mg) with indicated organic acids. The color code is shown at the bottom (with white color indicating no detectable activity). The heat map was generated using single matrix CIMminer [71]. Reaction conditions were as indicated in Materials and Methods.

Figure 6

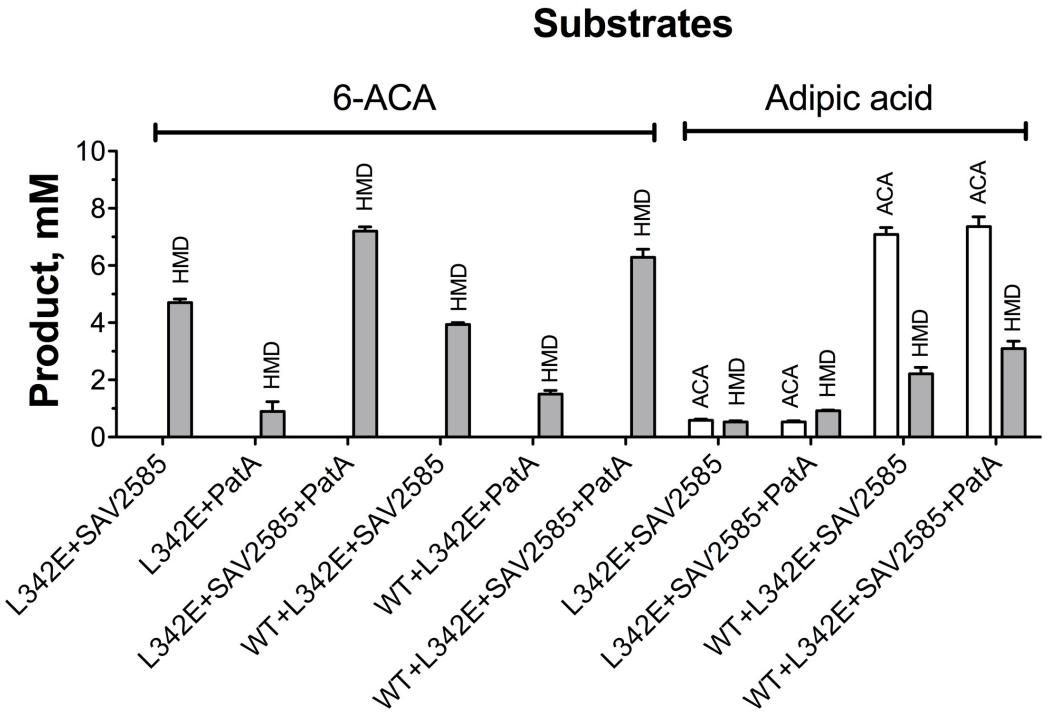

Figure 6. *In vitro* biotransformation of adipic acid (AA) and 6-aminocaproic acid (6-ACA) by purified wild type and mutant MAB4714 and ω-transaminases (ωTAs). Reaction mixtures (200 µl) contained 100 mM HEPES-K buffer (pH 7.5), 10 mM substrate (AA or 6-ACA), 2 mM NADPH, cofactor regeneration systems (2 mM ATP, 5 mM polyP, 10 mM $MgCl_2$, 0.05 mM PLP, 100 mM Na-formate, 50 mM NH_4Cl, 2 mM L-Glu, 20 µg of PPK2/CHU0107, 20 µg of the FDH D222Q/H224N protein, 20 µg of Glu-DH, and 20 µg of PPA), ωTAs (20 µg of SAV2585 or PatA), and 80 µg of purified wild type MAB4714 (WT) or L342E mutant protein (L342E) (overnight incubation at 30°C). Reaction products (6-ACA and 1,6-HMD) were analyzed using HPLC (C18 column) after O-phthalaldehyde derivatization of amine groups as described in Materials and Methods.